Ahmad *et al.*
Journal of the Egyptian National Cancer Institute (2024) 36:22
https://doi.org/10.1186/s43046-024-00227-1

Journal of the Egyptian National Cancer Institute

RESEARCH Open Access

Assessment of peripheral dose as a function of distance and depth from cobalt-60 beam in water phantom using TLD-100

Habib Ahmad[1], Javaid Ali[2*], Khalil Ahmad[3], Ghufran Biradar[1], Ashfaq Zaman[1], Yasir Uddin[4], Muhammad Sohail[5] and Shahid Ali[6]

Abstract

Background Innovations in cancer treatment have contributed to the improved survival rate of cancer patients. The cancer survival rates have been growing and nearly two third of those survivors have been exposed to clinical radiation during their treatment. The study of long-term radiation effects, especially secondary cancer induction, has become increasingly important. An accurate assessment of out-of-field/peripheral dose (PDs) is necessary to estimate the risk of second cancer after radiotherapy and the damage to the organs at risk surrounding the planning target volume. This study was designed to measure the PDs as a function of dose, distances, and depths from Teleco-balt-60 (Co-60) beam in water phantom using thermoluminescent dosimeter-100 (TLD-100).

Methods The PDs were measured for Co-60 beam at specified depths of 0 cm (surface), 5 cm, 10 cm, and 15 cm outside the radiation beam at distances of 5, 10, and 13 cm away from the radiation field edge using TLD-100 (G1 cards) as detectors. These calibrated cards were placed on the acrylic disc in circular tracks. The radiation dose of 2000 mGy of Co-60 beam was applied inside 10×10 cm^2 field size at constant source to surface distance (SSD) of 80 cm.

Results The results showed maximum and minimum PDs at surface and 5 cm depth respectively at all distances from the radiation field edge. Dose distributions out of the field edge with respect to distance were isotropic. The decrease in PDs at 5 cm depth was due to dominant forward scattering of Co-60 gamma rays. The increase in PDs beyond 5 cm depth was due to increase in the irradiated volume, increase in penumbra, increase in source to axis distance (SAD), and increase in field size due to inverse square factor.

Conclusion It is concluded that the PDs depends upon depth and distance from the radiation field edge. All the measurements show PDs in the homogenous medium (water); therefore, it estimates absorbed dose to the organ at risk (OAR) adjacent to cancer tissues/planning target volume (PTV). It is suggested that PDs can be minimized by using the SAD technique, as this technique controls sources of scattered radiation like inverse square factor and effect of penumbra up-to some extent.

Keywords Peripheral dose, TLD-100, Co-60 dosimetry, Depth dose, Penumbra

*Correspondence:
Javaid Ali
javaidalitarakai@gmail.com; javid.tarakai@yahoo.com
Full list of author information is available at the end of the article

Background

Radiation therapy (RT) is an effective treatment for cancer and the objectives of radiation therapy is to give the maximum radiation dose to the cancer tissues/target and minimum or no dose to the surrounding healthy tissues [1–3]. The number of radiotherapy cases are increasing day by day [4]. With the development/innovations in radiotherapy treatment modalities like 3D CRT, IMRT, VMAT SRS, SBRT, and IGRT with dose escalation and conformity of the target volume, there is increase in cure rats and patient surveillance [5]. The cancer surveillance has been increased, and nearly two third of these survivors are exposed to clinical radiation during their treatment [6]. The study of long-term radiation effects, especially the second cancer induction has become increasingly important. As many secondary cancers appears far from the target volume/PTV, therefore, the dose out of the field at peripheries (PD) should always be considered for theoretical assessment of secondary cancer risk [3, 7–9]. During radiotherapy treatment with high-energy photon beams, a small fraction of the delivered dose is absorbed a few centimeters away from the treatment beam/field [10]; this dose is known as peripheral dose (PD) and compared to high doses within the target volume. The associated cancer risk is likely to be much lower but not insignificant [11]. The risk of secondary cancer associated with low doses of ionizing radiation especially appears in long term survivors is gaining new interest every day [12]. Most of the secondary cancer within the margins of the treatment field (from 2.5 cm in to 5 cm out) has received a dose less than 6 Gy [13]. There is a 40% increase in solid tumor in lung after radiotherapy in prostate where the lung received a dose from 0.5 to 1.0 Gy [14]. Therefore, there is no dose that is regarded as safe. It is important to assess PDs to radiosensitive tissue/organs, such as the breast, gonads, and the thyroid to determine the possible risk of late effects, such as secondary cancers that could appear in long-term surviving patients (e.g., pediatric patients) [15]. PDs may also cause some radiation-induced diseases like cataract, infertility, lung fibrosis, and myocarditis and also contraindicated in pregnant patients [16]. In general, it is of extreme importance to calculate the PDs down to the level of 0.1% of the central axis maximum dose (d_{max}), and its determination has been the subject of extensive investigation [17]. The photon PDs has three sources: (a) leakage through the head shielding and the collimation systems; (b) scattering from the head and secondary collimators, and (c) scattering inside the patient/phantom [18]. Moreover, in the case of Co-60 unit, the penumbra due to source size is also an additional component of PDs. The scattering in the patient is the dominant source of the PD in regions close to the irradiated volume. However, its relative contribution to the total PDs rapidly decreases for further distances from the treatment edge, leaving collimator scattering and leakage as the predominant dose sources in those regions. At considerable distances, leakage is the only relevant dose source [19, 20]. Therefore, medical physicist is responsible to ensure that radio-sensitive tissues outside of the radiation beam do not receive doses approaching their tolerance levels. Detailed knowledge and accurate estimation of the magnitude and spatial distribution of the PDs is necessary, as this can be used in retrospective studies examining possible correlation between radiotherapy dose and secondary cancer incidence in radiotherapy patients [17]. It is also the responsibility of medical physicist to correctly estimate the radiation absorbed doses to OAR due to PDs and make accurate radiotherapy treatment plan [16].

There are no commercial treatment planning systems (TPSs) designed/available for the precise calculation of the PD and its significant deviations, compared to measurements and Monte Carlo (MC) simulations [21–23]. Several published mathematical models exist for estimating secondary cancer induction probability as a function of the radiation dose, which should count with an accurate out-of-field dose distribution received by the patient during RT [24–26]. The software Peri dose was probably the first attempt to calculate scattered dose outside the primary beam for individual treatments. However, it was only designed to be used for rectangular fields [10]. A simple and flexible analytical model for PDs estimation was also implemented into a computer program termed PERIPHOCAL, correctly predicted the PDs inside a humanoid phantom irradiated with IMRT and VMAT techniques. It presents, however, two main limitations: (a) the model was trained using only a few measurements points placed inside a humanoid phantom, and (b) it is one dimensional, i.e., it assumed that the organs were described only by the z coordinate of the organ and its length along the craniocaudal direction [27, 28]. Using complex mathematical functions to represent the physics behind each process and calculate the three peripheral dose components separately, a different approach to model peripheral dose was applied by Hauri et al. [29]. Other recently published models also considered calculating each contribution of the PDs separately. They did calculations in water cylinders with fast computation times but at the price of needing several fitting coefficients. Despite their high accuracy, the main disadvantage of those approaches is their complexity, which makes the clinical application very cumbersome [30, 31]. An attempt/study is to figure out the PD distribution outside of the radiation field at surface and depths using Co-60 teletherapy unit in our institute has been carried out.

In this study, TLD-100 (G1 cards), as a very effective tool for dose measurement [32], was used to measure the PDs received outside the treatment field at 5 cm, 10 cm, and 13 cm away from the field edge at surface (0 cm), 5 cm, 10 cm, and 15 cm depths in the water phantom. Also, the isotropic distribution of dose inside the tissue equivalent medium (water) from the source was carried out. Furthermore, the scattered to primary dose ratios at all depths and distances from the radiation field edges were estimated. Modern Co-60 teletherapy machines with the MLCs and 100 cm SSD are frequently in use for IMRT treatment. Intensity-modulated radiation therapy (IMRT) withCo-60 teletherapy [33, 34] can be suitable for complex superficial anatomic sites, and it can minimize the incidence of radiation toxicity in proximal organ at risk volume [35, 36]. Integrating technologies like multileaf collimator in Co-60 teletherapy [37–39] units can facilitate automated treatment [40, 41]. It is therefore important for medical physicists to consider the role of Co-60 teletherapy in advanced technologies like IMRT [41–43]. Co-60-based radiation therapy continues to play a significant role in not only developing countries where access to RT is extremely limited but also in industrialized countries [33, 34, 39, 44].

Therefore, from this study, the behavior of the Co-60 gamma ray beam inside the homogenous scattering medium was observed. By adding some useful techniques (factors), one can evaluate/estimate the radiation dose received by OAR, if the distance of the OAR is known outside the treatment field/volume, which is the significance of the study.

Methods

TLD-100 (G1 cards), Harshaw, USA, in disc shapes as shown in Fig. 1 were used in this study. The TLD-100 (G1) cards contained two chips in duplicate. These cards were first annealed and calibrated against a known dose from Co-60 source at Secondary Standard Dosimetry Laboratories (SSDL), Pakistan Institute of Nuclear Science and Technology (PINSTECH), Islamabad Pakistan. The calibration factor for each card is determined. The detectors were again annealed and irradiated from Co-60 teletherapy unit (Theratron Phoenix) at the Institute of Radiotherapy and Nuclear Medicines (IRNUM), Peshawar, Pakistan. The irradiation conditions were (a) field size of 10×10 cm^2 and (b) SSD of 80 cm. The radiation and reading time were fixed to be 48 h after irradiation in order to minimize the fading effect of the cards.

Dimensions of the cards were 3.1 mm × 3.1 mm × 0.89 mm and were encapsulated between two sheets of Teflon of 0.06 mm thickness. The cards of 8800 series manufactured with the card identification number in bar code format. A dedicated water phantom of dimension $35.5\times36\times36.5$ cm^3 with acrylic disc and isocentric tracks (provided by IAEA) [45] for TLD-100 (G1 cards) placement and radiation exposure was used for taking the data, as shown in the Fig. 2.

The reading of the TLD-100 (G1 cards) was carried out at Radiation Dosimetry Group (RDG) PINSTECH using a fully automatic and computerized thermoluminescence dosimetry workstation 8800 [46]. Thirty TLD-100 (G1) cards were annealed in Health Physics Division (HPD), PINSTECH. A total of 30 TLD-100 (G1 cards) were used; among these, only 20 random TLD-100 (G1 cards) were chosen in the experiment.

TLD-100 cards were placed in circular tracks of radii 10, 15, and 18 cm in such a way that in the first and second track there were 8 cards at 45° intervals. However, the outer third track contain 4 cards at 90° interval with all circular tracks outside radiation field(8 + 8 + 4) as shown in Fig. 2.

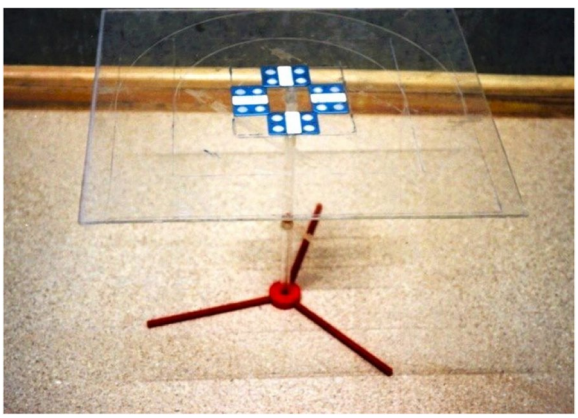

Fig. 1 Calibration of TLD cards inside the 10×10 cm^2 setup for dose measurement

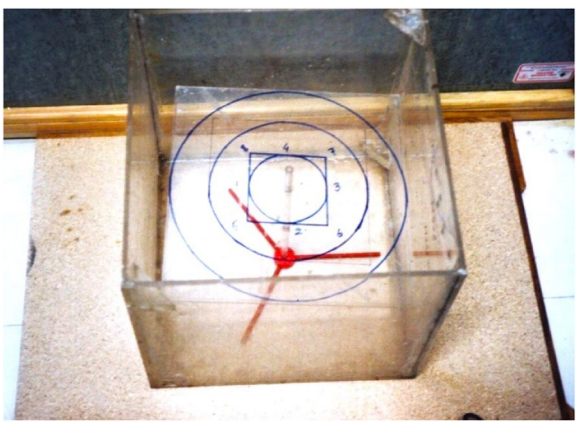

Fig. 2 Isocentric circles where TLD cards are placed outside the radiation field in the phantom

This assembly was placed on the surface of water phantom and the annealed cards were exposed to a dose of 2000 mGy from Co-60 gamma rays [46] in succession at a depth of 5 cm in water phantom. The calibration factor was calculated by Eq. 1.

$$CF = \frac{\text{Dose in mGy}}{\text{Response in nC}} \quad (1)$$

The exposed TLD-100 (G1 cards) was read out by taking four readings at each depth. In the whole experimental work, first TLD-100 (G1 cards) were read out and then again annealed, i.e., dual annealing was done, in order to avoid any residual peaks. In present work, the time interval of 48 h was fixed between the exposures and read out of TLD-100 (G1 cards, to maintain consistency in readings), using TRS-398 protocols [47]. To select the most reliable chip for the project work, F-test (statistical tool to compare the variance of two samples or the ratio of variances between multiple samples) was applied to check the most accurate chip response and found that the results of the chip-1 were more consistent than chip-1 [48]. Also, chip to chip calibration factor was available; therefore, it was better to use individual calibration factor for each chip-1. The PDs were measured for Co-60 beam at specified depths of 5, 10, and 15 cm outside the radiation beam at distances of 5, 10, and 13 cm away from the radiation field edge using TLD-100 (G1 cards). The isotropic distributions were confirmed and scattered to primary dose ratios were also estimated at the mentioned depths and distances from the radiation field edge in water phantom.

Results

Calibration factor for all chip-1 along with mean, standard deviation (SD), co-efficient of variation (COV), and mean deviation (MD) are shown in Table 1 and Fig. 3.

The mean CF, SD, MD, and COV for all chip-1 are 0.021633, 0.001236, 0.00173, and 5.7% respectively. The scatter to primary doses ratios at surface 0, 5, 10, and 15 cm depths and away from the radiation field at distances of 5, 10, and 13 cm as shown in Table 2 and Fig. 4.

PDs at various distances of 5, 10, and 13 cm away from radiation field edge along various depths of 0, 5, 10, and 15 cm with fixed SSD are shown in Table 3 and Fig. 5.

Discussion

Radiation therapy involves the delivery of a prescribed dose to the target volume, sparing the surrounding healthy organs and tissues as much as possible. Traditional techniques that ensure the prescribed dose gets delivered to the target volume include treatment planning systems and water/humanoid phantom studies.

Table 1 Mean, standard deviations, coefficient of variation, and calibration factors for all chips (chip-1)

S.No	CF	TLD ID	S.No	CF	TLD ID
1	0.023479	423	**16**	0.021831	474
2	0.020821	424	**17**	0.02103	478
3	0.021465	425	**18**	0.021476	479
4	0.023394	426	**19**	0.021981	481
5	0.020378	427	**20**	0.022964	482
6	0.020165	428	**21**	0.022157	483
7	0.021368	429	**22**	0.023163	484
8	0.021482	430	**23**	0.02182	485
9	0.019722	431	**24**	0.020663	487
10	0.020069	437	**25**	0.021514	488
11	0.024131	439	**26**	0.022444	489
12	0.023471	468	**27**	0.022842	491
13	0.020391	469	**28**	0.022457	492
14	0.019611	470	**29**	0.021234	493
15	0.019883	471	**30**	0.021595	495
Mean			0.021633		
SD			0.001236		
MD			0.00173		
CV			5.7%		

These dose monitoring methods are done before the radiation treatment for radiation dose delivery verification as a quality assurance tool and may reflect the radiation dose delivered during treatment. In the current study, dose was measured in the water phantom using TLD-100 (G1 cards) as detectors out of the irradiated field as PDs. The measured PDs provides dose distribution in the homogenous medium outside the irradiated volume; therefore, it estimates dose to the OAR in radiotherapy patients. The PDs along the horizontal distance showed strong dependency on the distance from the radiation field edge and follows an exponential decrease along the surface and can be assumed to dose received on the surface. The dose at depth in water phantom shows the dose distribution inside the scattering medium. The PDs at 5, 10, and 13 cm away in circular track confirmed the isotropic distribution of radiation dose from Co-60 source along the depth and surface. The scattered to primary dose ratios were 11.69%, 6.53%, and 4.43% at 5, 10, and 13 cm away from the treatment field edge respectively on the surface. % PD is higher on the phantom surface. The surface dose was observed high due to contribution from all the scattering components of the Co-60 machine [49, 50]. The PDs recorded at 5 cm depth and 5, 10, and 13 cm away from the field edge was the least. Scattered to primary dose ratios at these positions were 3.89%, 1.44%, and 0.83% respectively. Internal scattered radiation is the predominant source of PDs. The depth dependence

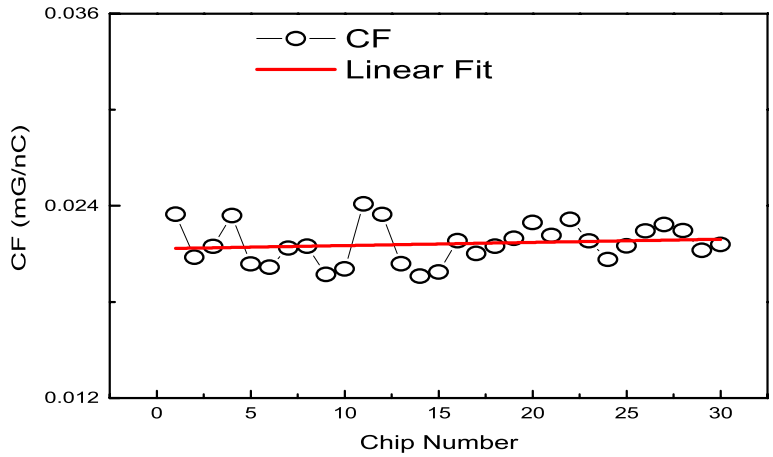

Fig. 3 Chip-1 calibration factors and its deviation

Table 2 Scatter to primary doses ratios at various depths along the various distances from the radiation field edge

Depth (cm)	Scatter/primary (ratio) 5 cm away	Scatter/primary (ratio) 10 cm away	Scatter/primary (ratio) 13 cm away
0	11.69%	6.54%	4.43%
5	3.9%	1.44%	0.83%
10	6.4%	2.237%	1.27%
15	9.8%	5.96%	3.2%

Table 3 PDs at varying depths and distances away from the radiation field edge at constant SSD

Distance	Surface(0 depth) dose (mGy)	5 cm depth dose (mGy)	10 cm depth dose (mGy)	15 cm depth dose (mGy)
5	114.028	61.36	72.71	77.5
10	64.09	22.76	25.36	46.93
13	43.406	13.095	14.25	25.3

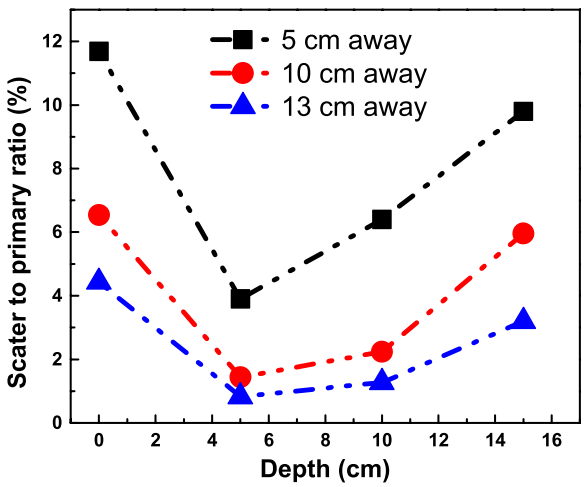

Fig. 4 The scatter to primary doses ratios at various depths and various distances from the radiation field edge

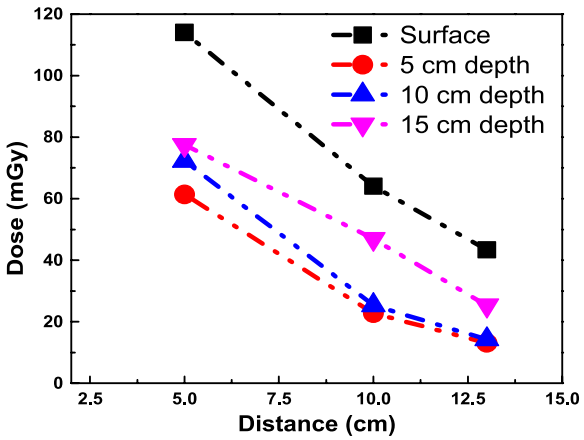

Fig. 5 PDs at various depths and various distances away from the radiation field edges at constant SSD

is determined by the attenuation of the primary photons; the reason of these least PDs is least scattering due to contribution from the collimator, phantom material, and other sources such as leakage and penumbra of Co-60 source having insufficient energy to reach the detectors at these points. The second reason behind this behavior is also the dominant forward scattering of cobalt-60 gamma rays [49, 50] and least scattering towards the sides at this depth. Also, the behavior of the PDs around the source was noted as isotropic. The PDs recorded at 10 and 15 cm depths showed clear increase in PDs than at 5 cm depth and is approximately doubled and tripled,

respectively. The PDs decreases almost exponentially with the increase of distance from the field edge at these depths. The scatter to primary dose ratios at 5, 10, and 13 cm away from the radiation field edge at these depths (10 and 15 cm) were 6.4% and 9.8%, 2.25% and 5.95%, and 1.26% and 3.21%, respectively as shown in Table 2. The change in trend/increase in the PDs at these depths have several reasons like (a) scattering medium; (b) increased irradiated volume; (c) increase in penumbra; (d) increase SAD as SSD was fixed in the study, i.e., inverse square factor; (e) less forward scattering of Co-60 beam; and (f) increase inside and back scattering. So, all these factors contributed in increase in scattered dose [49].

This experimental study confirmed that the dose distribution is isotropic, so the PDs at any depths and distance can be estimated by applying proper interpolation that will be helpful to estimate the absorbed dose to OARs in RT of cancer patients. Accordingly, that will be used in retrospective/prospective studies examining possible correlation between RT recommended dose and secondary cancer incidence/risk. It also leads to an accurate assessment of out-of-field dose/PD necessary to estimate the risk of second cancer after radiotherapy and the damage to the organs at risk surrounding the planning target volume.

Conclusion

It is concluded that measured PDs in water phantom as a homogenous medium estimates the absorbed dose to OARs in radiotherapy of cancer patients. The PDs as a function of distance and depths showed strong dependency on radiation dose given, depth in tissue, distance from the target volume, SAD, inverse square factor, penumbra, irradiated volume, collimator scattering, leakage from the source housing, and scattered radiation in the tissue. The increase of PDs along the surface and depth beyond 5 cm do not recommend the use of Co-60 unit for treatment of superficial and deep-seated tumors at greater depths, i.e., beyond 5 cm using single field. It is suggested that the PDs can be minimized by using the isocentric technique and multiple fields with beam weighting as these techniques controls sources of scattered radiation like inverse square factor, given the dose and effect of penumbra up to some extent especially in patients having long-term surveillance expectancy. Special attention is required for tumors near moving organs like the lungs and diaphragm.

Abbreviations

SD Standard deviation
COV Coefficient of variation
MD Mean deviation
SSD Source to surface distance
SAD Source to axis distance
PD Peripheral dose
CF Calibration factor
TLD Thermoluminescent detector

Acknowledgements

The authors are giving credit or appreciation to the Pakistan Institute of Science and Technology (PINSTECH) Islamabad and Institute of Radiotherapy and Nuclear Medicines (IRNUM) cancer hospital, Peshawar, Pakistan, that already supports this research and publication.

Authors' contributions

The idea, study design, and data manipulation represented the role of HA, JA, and KA. Statistical analyses, table and figure preparation, and interpretation were done by JA, HA, and SA. Data collection was done by HA, GB, KA, and AZ. YU, JA, and MS were responsible for proofreading. All the authors have contributed in the interpretation of data and the manuscript preparation. The authors read and approved the final manuscript.

Funding

None declared.

Availability of data and materials

The datasets used and analyzed in this study are available from the corresponding author upon reasonable request.

Declarations

Ethics approval and consent to participate

Not applicable.

Consent for publication

Not applicable.

Competing interests

The authors declare that they have no competing interests.

Author details

[1]Swat Institute of Nuclear Medicine, Oncology & Radiotherapy (SINOR) Cancer Hospital, Saidu Sharif Swat, KPK, Pakistan. [2]Larkana Institute of Nuclear Medicine and Radiotherapy (LINAR) Cancer Hospital, Larkana, Sindh, Pakistan. [3]Pakistan Institute of Nuclear Science and Technology (PINSTECH), Islamabad, Pakistan. [4]Royal College of Nursing, Saidu Sharif, Swat, KPK, Pakistan. [5]International Collaborative Laboratory of 2D Materials for Optoelectronics Science and Technology of Ministry of Education, Institute of Microscale Optoelectronics, College of Electronics and Information Engineering, Shenzhen University, Shenzhen 518060, China. [6]Department of Physics, University of Peshawar (UOP), Peshawar, KPK, Pakistan.

Received: 26 October 2023 Accepted: 8 May 2024
Published online: 24 June 2024

References

1. Acharya NP, Lamichhane TR, Jha B. Quality assurance with dosimetric consistency of a Co-60 teletherapy unit. J Nepal Phys Soc. 2017;4(1):88–92.
2. Dracham CB, Shankar A, Madan R. Radiation induced secondary malignancies: a review article. Radiat Oncol J. 2018;36(2):85.
3. Mazonakis M, Damilakis J. Out-of-field organ doses and associated risk of cancer development following radiation therapy with photons. Physica Med. 2021;90:73–82.
4. Schneider CW. Stray radiation dose from X-ray and proton beam radiation therapies. LSU Doctoral Dissertations; 2019. p, 4971. https://repository.lsu.edu/gradschool_dissertations/4971.
5. Society AC. Cancer treatment and survivorship facts & figures 2014–2015. Atlanta: American Cancer Society; 2014. p. 2014.
6. Newhauser W. Physician characteristics and distribution in the US: American Medical Association Press; 1999.

7. Council NR. Health risks from exposure to low levels of ionizing radiation: BEIR VII phase 2. 2006. https://doi.org/10.31390/gradschool_dissertations.4971.
8. De Gonzalez AB, Apostoaei AI, Veiga LH, Rajaraman P, Thomas BA, Hoffman FO, et al. RadRAT: a radiation risk assessment tool for lifetime cancer risk projection. J Radiol Prot. 2012;32(3):205.
9. Taddei PJ, Khater N, Zhang R, Geara FB, Mahajan A, Jalbout W, et al. Inter-institutional comparison of personalized risk assessments for second malignant neoplasms for a 13-year-old girl receiving proton versus photon craniospinal irradiation. Cancers. 2015;7(1):407–26.
10. van der Giessen P-H. Peridose, a software program to calculate the dose outside the primary beam in radiation therapy. Radiother Oncol. 2001;58(2):209–13.
11. Vlachopoulou V, Malatara G, Delis H, Theodorou K, Kardamakis D, Panayiotakis G. Peripheral dose measurement in high-energy photon radiotherapy with the implementation of MOSFET. World journal of radiology. 2010;2(11):434.
12. Brenner DJ, Doll R, Goodhead DT, Hall EJ, Land CE, Little JB, et al. Cancer risks attributable to low doses of ionizing radiation: assessing what we really know. Proc Natl Acad Sci. 2003;100(24):13761–6.
13. Dörr W, Herrmann T. Cancer induction by radiotherapy: dose dependence and spatial relationship to irradiated volume. J Radiol Prot. 2002;22(3A):A117.
14. Brenner DJ, Curtis RE, Hall EJ, Ron E. Second malignancies in prostate carcinoma patients after radiotherapy compared with surgery. Cancer. 2000;88(2):398–406.
15. Brenner DJ, Sachs RK. Estimating radiation-induced cancer risks at very low doses: rationale for using a linear no-threshold approach. Radiat Environ Biophys. 2006;44:253–6.
16. Shahban M, Hussain B, Mehmood K, Rehman SU. Estimation of peripheral dose from Co beam in water phantom measured in Secondary Standard Dosimetry Laboratory, Pakistan. Rep Pract Oncol Radiother. 2017;22(3):212–6.
17. McParland BJ, Fair HI. A method of calculating peripheral dose distributions of photon beams below 10 MV. Med Phys. 1992;19(2):283–93.
18. Kase KR, Svensson GK, Wolbarst AB, Marks MA. Measurements of dose from secondary radiation outside a treatment field. Int J Radiat Oncolo Biol Phys. 1983;9(8):1177–83.
19. Ruben JD, Lancaster CM, Jones P, Smith RL. A comparison of out-of-field dose and its constituent components for intensity-modulated radiation therapy versus conformal radiation therapy: implications for carcinogenesis. Int J Radiat Oncol Biol Phys. 2011;81(5):1458–64.
20. Stovall M, Blackwell CR, Cundiff J, Novack DH, Palta JR, Wagner LK, et al. Fetal dose from radiotherapy with photon beams: report of AAPM Radiation Therapy Committee Task Group No. 36. Med Phys. 1995;22(1):63–82.
21. Sánchez-Nieto B, Medina-Ascanio KN, Rodríguez-Mongua JL, Doerner E, Espinoza I. Study of out-of-field dose in photon radiotherapy: a commercial treatment planning system versus measurements and Monte Carlo simulations. Med Phys. 2020;47(9):4616–25.
22. Howell RM, Scarboro SB, Kry S, Yaldo DZ. Accuracy of out-of-field dose calculations by a commercial treatment planning system. Phys Med Biol. 2010;55(23):6999.
23. Azab H, Moussa R, Kamaleldin M. Peripheral photon doses from different techniques delivered in prostate radiotherapy: experimental measurements and TPS calculations. Arab J Nucl Sci Appl. 2020;53(1):67–75.
24. Sánchez-Nieto B, Romero-Expósito M, Terrón JA, Sánchez-Doblado F. Uncomplicated and Cancer-Free Control Probability (UCFCP): a new integral approach to treatment plan optimization in photon radiation therapy. Physica Med. 2017;42:277–84.
25. Schneider U. Modeling the risk of secondary malignancies after radiotherapy. Genes. 2011;2(4):1033–49.
26. Hall EJ, Wuu C-S. Radiation-induced second cancers: the impact of 3D-CRT and IMRT. Int J Radiat Oncol Biol Phys. 2003;56(1):83–8.
27. Sánchez-Nieto B, El-Far R, Irazola L, Romero-Expósito M, Lagares J, Mateo J, et al. Analytical model for photon peripheral dose estimation in radiotherapy treatments. Biomed Phys Eng Express. 2015;1(4):045205.
28. Sánchez-Nieto B, Irazola L, Romero-Expósito M, Terrón J, Sánchez-Doblado F. PO-0808: validation of a clinical peripheral photon dose model: prostate IMRT irradiation of Alderson phantom. Radiother Oncol. 2016;1(119):S381–2.
29. Hauri P, Hälg RA, Besserer J, Schneider U. A general model for stray dose calculation of static and intensity-modulated photon radiation. Med Phys. 2016;43(4):1955–68.
30. Schneider CW, Newhauser WD, Wilson LJ, Kapsch R-P. A physics-based analytical model of absorbed dose from primary, leakage, and scattered photons from megavoltage radiotherapy with MLCs. Phys Med Biol. 2019;64(18):185017.
31. Wilson LJ, Newhauser WD, Schneider CW, Kamp F, Reiner M, Martins JC, et al. Method to quickly and accurately calculate absorbed dose from therapeutic and stray photon exposures throughout the entire body in individual patients. Med Phys. 2020;47(5):2254–66.
32. Chen YS, Wu SW, Huang HC, Chen HH. Absolute dose measurement and energy dependence of LiF dosimeters in proton therapy beam dosimetry. Therapeutic Radiol Oncol. 2022;6. https://doi.org/10.21037/tro-22-16.
33. Adams E, Warrington A. A comparison between cobalt and linear accelerator-based treatment plans for conformal and intensity-modulated radiotherapy. Br J Radiol. 2008;81(964):304–10.
34. Ravichandran R. Has the time come for doing away with cobalt-60 teletherapy for cancer treatments. J Med Phys Assoc Medi Phys India. 2009;34(2):63.
35. Bucci MK, Bevan A, Roach M III. Advances in radiation therapy: conventional to 3D, to IMRT, to 4D, and beyond. CA Cancer J Clin. 2005;55(2):117–34.
36. van der Molen L, Heemsbergen WD, de Jong R, van Rossum MA, Smeele LE, Rasch CR, et al. Dysphagia and trismus after concomitant chemo-Intensity-Modulated Radiation Therapy (chemo-IMRT) in advanced head and neck cancer; dose–effect relationships for swallowing and mastication structures. Radiother Oncol. 2013;106(3):364–9.
37. Joshi CP, Dhanesar S, Darko J, Kerr A, Vidyasagar P, Schreiner LJ. Practical and clinical considerations in cobalt-60 tomotherapy. J Med Phys Assoc Med Phys India. 2009;34(3):137.
38. Joshi CP, Darko J, Vidyasagar P, Schreiner LJ. Investigation of an efficient source design for cobalt-60-based tomotherapy using EGSnrc Monte Carlo simulations. Phys Med Biol. 2008;53(3):575.
39. Omer MAA. Partial quality assessment of 60Co-teletherapy machine performance. Open J Radiol. 2015;5(04):235.
40. Fox C, Romeijn HE, Lynch B, Men C, Aleman DM, Dempsey JF. Comparative analysis of 60Co intensity-modulated radiation therapy. Phys Med Biol. 2008;53(12):3175.
41. Kerr A, Rawluk N, MacDonald A, Marsh M, Schreiner J, Darko J. Cobalt-60 source based image guidance in broad beam cobalt-60 IMRT. Int J Radiat Oncol Biol Phys. 2010;78(3):S701.
42. Cadman P, Bzdusek K. Co-60 tomotherapy: a treatment planning investigation. Med Phys. 2011;38(2):556–64.
43. Elhassan SE. Evaluation of motorized wedge for a new generation telecobalt machine. 2008.
44. Salminen EK, Kiel K, Ibbott GS, Joiner MC, Rosenblatt E, Zubizarreta E, et al. International Conference on Advances in Radiation Oncology (ICARO): outcomes of an IAEA meeting. Radiat Oncol. 2011;6:1–10.
45. Izewska J, Georg D, Bera P, Thwaites D, Arib M, Saravi M, et al. A methodology for TLD postal dosimetry audit of high-energy radiotherapy photon beams in non-reference conditions. Radiother Oncol. 2007;84(1):67–74.
46. Liu C-j, Sims C, Rhea T. Optimization of the readout procedures for the Harshaw 8800 TL (thermoluminescent) dosimetry system. Oak Ridge National Lab.(ORNL), Oak Ridge, TN (United States), 1989.
47. Izewska J, Hultqvist M, Bera P. Analysis of uncertainties in the IAEA/WHO TLD postal dose audit system. Radiat Meas. 2008;43(2–6):959–63.
48. Kirkwood BR. Essentials ofMedical Statistics. Boston, Mass: Black-well Scientific Publications; 1988.
49. Kinhikar RA. Surface dose for five telecobalt machines, 6MV photon beam from four linear accelerators and a Hi-Art Tomotherapy. Technol Cancer Res Treat. 2008;7(5):381–4.
50. Ravichandran R. Radioactive cobalt-60 teletherapy machine–estimates of personnel dose in mock emergency in patient release during "source stuck situation." J Med Phys. 2017;42(2):96.

Publisher's Note